American Journal of Pathology, Vol. 156, No. 6, June 2000

Treatment-Induced Decline of Human Immunodeficiency Virus-1 p24 and HIV-1 RNA in Lymphoid Tissue of Patients with Early Human Immunodeficiency Virus-1 Infection

Herbert Kuster,* Milos Opravil,* Peter Ott,† Erika Schlaepfer,* Marek Fischer,* Huldrych F. Günthard,* Ruedi Lüthy,* Rainer Weber,* and Richard W. Cone*

From the Division of Infectious Diseases, Department of Internal Medicine, and the Policlinic for Ear, Nose, Throat and Face Surgery,† University Hospital Zurich, Zurich, Switzerland*

We report detailed quantitative analysis of human immunodeficiency virus-1 (HIV-1) p24 and HIV-1 RNA in tonsil biopsies from 13 patients with early, asymptomatic HIV infection before and during combination antiretroviral therapy. Using fluorescent microscopy in conjunction with reverse transcriptase-polymerase chain reaction of frozen tissue sections, we show that plasma and tissue viral loads decreased by approximately 3 logs during the 1-year treatment period, with good correlation between the HIV-1 p24 and HIV-1 RNA response in tissue. The decrease of tissue viral load was delayed compared to plasma viral load, possibly explained by the observation that the amount of follicular dendritic cell-associated virus correlated best with the area under the curve of plasma HIV-1 RNA throughout the last 12 weeks. Before and during treatment, the relative proportions of HIV-1 on follicular dendritic cells and within mononuclear cells remained constant, suggesting similar decay characteristics in these two lymphoid tissue compartments. However, viral p24 or RNA remained almost always detectable in tissue despite full suppression of HIV-1 RNA in plasma, and increased even after short-term rebounds in plasma viral load. Thus, full and sustained suppression of viral replication was required to efficiently decrease viral load in lymphoid tissue, but complete abolition of residual viral replication was not achieved. ***(Am J Pathol 2000, 156:1973–1986)***

Lymphoid tissue is the major reservoir of human immunodeficiency virus-1 (HIV-1) and the main site for virus propagation *in vivo*.[1,2] Infected CD4-positive T cells, most of which also reside in lymphoid tissue,[3] are the cell type that is predominantly responsible for high-level replication of HIV-1. Several studies have shown that substantial decreases in lymphoid tissue viral load (VL) occur in HIV-infected individuals who are successfully treated with combinations of antiretroviral drugs.[4–6] However, residual cell-free and cell-associated HIV-1 RNA remains present in virtually every patient despite effective and potent antiretroviral therapy, representing low-level viral replication[7] or viral transcription in long-lived HIV infected cells.[8–11] Although peripheral blood mononuclear cell-associated HIV-1 RNA may be a reasonable indicator of the overall VL in lymphoid tissue,[12] little knowledge still exists regarding the quantitative distribution of HIV-1 in lymphoid tissue and the corresponding kinetics in response to the initiation of antiretroviral therapy, particularly in patients with early HIV infection.

Only a small fraction of HIV-1 in lymphoid tissue is actually associated with productively infected lymphocytes.[3,13,14] Most of the lymphoid tissue-associated virus is concentrated on the surface of follicular dendritic cells (FDC), where it is thought to be trapped by complement receptors that capture complement-tagged virus or virus-antibody immune complexes,[3,15–17] or other mechanisms depending on cellular adhesion molecules.[18] A portion of FDC-trapped virus probably remains infectious,[14,15,18] and some researchers have reported evidence for productive infection of FDC.[19–21]

Different methods have previously been applied to analyze VL *in situ*, visualizing either HIV-1 RNA by *in situ*

Supported by Swiss National Science Foundation (grants 32–43654 and 32–46016), the Swiss HIV Cohort Study (project no. 144; Swiss Federal Office of Public Health grant 3600.010.1), Glaxo Wellcome, and Abbott Laboratories.

Accepted for publication February 9, 2000.

The members of the Swiss HIV Cohort Study are M. Battegay (Chairman of the Scientific Board), E. Bernasconi, Ph. Bürgisser, M. Egger, P. Erb, W. Fierz, M. Flepp (Chairman of the Group Clinics), P. Francioli (President of the SHCS, Centre Hospitalier Universitaire Vaudois, CH-1011- Lausanne), H.J. Furrer, P. Grob, B. Hirschel, B. Ledergerber, L. Matter (Chairman of the Group Laboratories), A. Meynard, M. Opravil, F. Paccaud, G. Pantaleo, L. Perrin, W. Pichler, J-C. Piffaretti, M. Rickenbach (Head of Coordination and Data Center), C. Rudin, P. Sudre, J. Schüpbach, A. Telenti, P. Vernazza, and R. Weber.

Address reprint requests to Herbert Kuster, University Hospital, Division of Infectious Diseases, Department of Internal Medicine, CH-8091 Zurich, Switzerland. E-mail: herbert.kuster@dim.usz.ch.

hybridization (ISH) or the viral capsid protein p24 using immunohistochemistry (IHC), allowing to differentiate between the intracellular and extracellular fractions of HIV-1. Most previous studies on histological HIV-1 detection involved the use of formalin-fixed, paraffin-embedded tissues.[4,22,23] Some of the most sensitive, quantitative ISH methods used radioactively-labeled nucleic acid probes for hybridization and photographic emulsion overlays for detection, resulting in a lower detection limit of approximately 20 HIV-1 RNA copies per cell.[3,24–27] Nonradioactive ISH methods for HIV-1 RNA detection, involving bright-field microscopy of enzymatically-deposited visible products, have generally been less sensitive and may miss FDC-associated virions.[28,29] Nonradioactive IHC detection with anti-p24 antibodies typically reveals more HIV-1 than nonradioactive ISH, and has been shown to reveal FDC-associated virus.[22,24] Nonradioactive ISH and IHC methods have been especially useful for co-localizing HIV-1 with cell surface markers, which is usually accomplished by two-color reactions.[19,30]

Protein or nucleic acid targets can also be visualized using well-established fluorescent microscopy methods.[21,31–35] With recent applications of ultra-sensitive digital cameras, high-yield fluorescent reagents and image analysis software, fluorescent microscopy is emerging as an extremely sensitive alternative to radioactive detection methods. By avoiding emulsion overlays, fluorescent methods offer improved flexibility for multicolor detection and simultaneous co-localization and were therefore used in this study.

This article reports detailed analyses of HIV-1 in lymphoid tissues using highly sensitive, quantitative detection of HIV-1 p24 and HIV-1 RNA by fluorescent microscopy. Quantitative IHC and ISH fluorescent measurements were corroborated by comparison with results from a recently developed HIV-1 reverse transcriptase-polymerase chain reaction (RT-PCR) assay for tissues.[36] The comparison was made possible by using a novel tissue-sectioning strategy resulting in serial, unfixed frozen tissue sections. These techniques enabled us to analyze the cell-associated distribution of HIV-1 in lymphoid tissue from HIV-1-infected individuals, both before and after the initiation of antiretroviral therapy, and to assess the kinetics of HIV-1 decay in four sequential tonsil biopsies.

Materials and Methods

Patients and Specimen Collection

Within the framework of a larger clinical study,[37] 13 asymptomatic, antiretroviral-naive, HIV-1-infected individuals with >400 CD4 cells per μl at entry were randomized to receive double therapy with AZT and 3TC or triple therapy with AZT, 3TC, and ritonavir and underwent sequential tonsil biopsies (Table 1). The study was approved by the Zurich University Hospital Ethics Committee and all participants provided signed consent. The study protocol called for each patient to come for monthly follow-up visits including collection of blood specimens and to donate four sequential palatine tonsil biopsies at weeks 0 (pretherapy), 4, 24, and 48 (on therapy); 50 out of 52 planned biopsies were obtained. Biopsies ($\sim$2 $\times$ 2 $\times$ 4 mm in size) were excised using 4-mm Takahashi forceps and immediately placed in a screw-top tube containing 0.5 ml of sterile Hanks' buffered salt solution. Specimens were submerged in liquid nitrogen within 2 minutes of excision. Of eight patients starting with triple therapy (triple-therapy group), one switched to double therapy at week 13 because of intolerance of ritonavir; of five patients starting double therapy (double-therapy group), two switched to triple therapy at weeks 24 or 40, respectively.

Sectioning Strategy

Each tonsil biopsy was entirely cryosectioned (6 μm; cryostat CM3050, Leica, Wetzlar, Germany) and each series of 18 consecutive sections was defined as one level. Per biopsy, $\sim$20 to 40 levels were generated. The 18 sections from each level were serially distributed as follows: four sections for IHC, four sections for ISH, one section for hematoxylin and eosin (H&E) staining, three sections for RNA extraction, three sections for DNA extraction, and three sections for backup. Frozen sections (6 μm) used for histology or histochemistry were put on Superfrost Plus slides (Gerhard Menzel Glasbearbeitungswerk GmbH & Co. kg, Braunschweig, Germany) kept at room temperature, dried for 2 minutes at 50°C, and stored at $-$70°C in individual air-tight bags. Sections for bulk extractions from each level were combined in separate tubes and stored at $-$70°C.

Morphometry

To assess total tissue area and lymphoid tissue area, computer-aided morphometry (AxioHOME; Zeiss, Oberkochen, Germany) was performed on one section from each level stained by H&E. Areas were converted to weight using the thickness of sections (6 μm) and assuming a density of 1 mg/mm^3. The calculated average total tissue weight (50 biopsies) was 6.65 mg/biopsy (SD, 2.72).

Immunohistochemistry

Slides with frozen sections were brought to room temperature, fixed for 10 minutes in 3% paraformaldehyde/phosphate buffered saline (PBS) at room temperature, and subsequently washed twice in PBS. Sections were equilibrated in TNT (100 mmol/L Tris, 150 mmol/L NaCl, 0.05% Tween 20, pH 7.5), then covered with 100 μl TNB (100 mmol/L Tris, 150 mmol/L NaCl, 0.5% blocking reagent, pH 7.5; NEN, Boston, MA) for 30 minutes and then sequentially covered with 75 μl TNB containing: 1) mouse anti-HIV-1 p24 diluted 1:10 (DAKO Diagnostics AG, Zug, Switzerland) and rabbit anti-CD3 (1:200; DAKO); 2) 5 μg/ml of Cy3-conjugated goat anti-mouse immunoglobulin (Ig) (Amersham, Little Chalfont, GB) and 5 μg/ml Alexa 488-conjugated goat anti-rabbit Ig (Molecular Probes Europe BV, Leiden, The Netherlands); 3) 5 μg/ml of mouse IgG (Sigma, Buchs, Switzerland); 4) mouse IgM

Table 1. Sequential Measurements of Tonsil HIV-1 p24 and HIV-1 RNA in Patients under Combination Antiretroviral Therapy

Patient Group*	Week	Treatment (week of change)	Total tonsil HIV-1 p24 (FI/100ng LT)	Number of p24 positive cells (cells/mg LT)	RT-PCR tonsil (copies/mg LT)	ISH (Granule count per mg LT)	Plasma VL (copies/ml)
101	0	none	$3.08 \cdot 10^5$	126	$5.14 \cdot 10^6$	$1.86 \cdot 10^5$	$3.26 \cdot 10^4$
A	4	AZT+3TC+RIT	$5.43 \cdot 10^5$	295	$1.81 \cdot 10^5$	$5.48 \cdot 10^4$	$2.90 \cdot 10^1$
	24	AZT+3TC+RIT	<1300	<130	<462	<4330	<16
	48	AZT+3TC+RIT	<140	<14	<149	<1210	<8
103	0	none	$2.60 \cdot 10^5$	<9	$1.15 \cdot 10^5$	$5.96 \cdot 10^3$	$6.15 \cdot 10^3$
A	4	AZT+3TC+RIT	$1.87 \cdot 10^5$	<13	$1.92 \cdot 10^3$	<1290	<13
	24	AZT+3TC (13)	$3.13 \cdot 10^5$	<7	$7.25 \cdot 10^2$	<669	<19
	48	AZT+3TC	n.d.	n.d.	n.d.	n.d.	<5
118	0	none	$3.27 \cdot 10^6$	226	$6.66 \cdot 10^5$	$3.62 \cdot 10^5$	$3.14 \cdot 10^4$
A	4	AZT+3TC+RIT	$1.46 \cdot 10^6$	<28	$6.55 \cdot 10^4$	$6.87 \cdot 10^4$	$2.93 \cdot 10^2$
	24	AZT+3TC+RIT	$1.10 \cdot 10^5$	<11	$9.69 \cdot 10^2$	<1070	<14
	48	AZT+3TC+RIT	<758	<76	$1.04 \cdot 10^3$	<7580	<7
121	0	none	$1.39 \cdot 10^6$	145	$5.03 \cdot 10^5$	$5.91 \cdot 10^4$	$1.25 \cdot 10^4$
A	4	AZT+3TC+RIT	$4.94 \cdot 10^5$	90	$8.74 \cdot 10^4$	$2.48 \cdot 10^4$	$9.03 \cdot 10^3$
	24	AZT+3TC+RIT	$2.32 \cdot 10^4$	<12	$5.39 \cdot 10^2$	<1500	<10
	48	AZT+3TC+RIT	$1.38 \cdot 10^5$	53	$1.66 \cdot 10^3$	<934	<19
126	0	none	$1.30 \cdot 10^6$	179	$4.29 \cdot 10^5$	$8.79 \cdot 10^4$	$2.59 \cdot 10^3$
A	4	AZT+3TC+RIT	$5.54 \cdot 10^4$	<6	$5.50 \cdot 10^3$	$1.55 \cdot 10^4$	$4.40 \cdot 10^1$
	24	AZT+3TC+RIT	<50	<5	$1.78 \cdot 10^2$	<498	<9
	48	AZT+3TC+RIT	$4.12 \cdot 10^3$	<6	$3.11 \cdot 10^1$	<584	<8
402	0	none	$7.30 \cdot 10^5$	228	$1.76 \cdot 10^5$	$5.24 \cdot 10^4$	$2.00 \cdot 10^4$
A	4	AZT+3TC+RIT	$9.14 \cdot 10^3$	<17	$2.87 \cdot 10^3$	<1740	$1.06 \cdot 10^2$
	24	AZT+3TC+RIT	<401	<40	$1.77 \cdot 10^2$	<4010	$3.20 \cdot 10^1$
	48	AZT+3TC+RIT	<199	<20	$7.34 \cdot 10^1$	<1990	<12
124	0	none	$2.56 \cdot 10^5$	71	$1.50 \cdot 10^5$	$5.76 \cdot 10^3$	$1.36 \cdot 10^4$
A	4	AZT+3TC+RIT	$1.42 \cdot 10^5$	<9	$5.92 \cdot 10^3$	$4.46 \cdot 10^4$	$1.58 \cdot 10^3$
	24	AZT+3TC+RIT	<61	<6	$1.40 \cdot 10^2$	<610	$1.69 \cdot 10^2$
	48	AZT+3TC+RIT	<50	<5	$5.58 \cdot 10^1$	<505	9
109	0	none	$2.91 \cdot 10^6$	172	$3.96 \cdot 10^5$	$2.13 \cdot 10^5$	$1.68 \cdot 10^5$
B	4	AZT+3TC	$5.85 \cdot 10^6$	406	$4.17 \cdot 10^4$	$8.98 \cdot 10^4$	$1.93 \cdot 10^2$
	24	AZT+3TC	$4.37 \cdot 10^5$	<40	$4.84 \cdot 10^4$	$1.51 \cdot 10^5$	$2.50 \cdot 10^4$
	48	ddI+d4T+RTV (24)	$1.12 \cdot 10^3$	<21	$1.06 \cdot 10^2$	$1.01 \cdot 10^5$	<6
112	0	none	$2.49 \cdot 10^4$	<9	$3.06 \cdot 10^5$	$1.72 \cdot 10^4$	$9.13 \cdot 10^4$
B	4	AZT+3TC	$1.26 \cdot 10^4$	208	$1.35 \cdot 10^4$	<6310	$1.03 \cdot 10^3$
	24	AZT+3TC	$4.20 \cdot 10^5$	<4	$2.01 \cdot 10^5$	$1.59 \cdot 10^5$	$1.39 \cdot 10^3$
113	0	none	$4.53 \cdot 10^6$	171	$4.21 \cdot 10^5$	$2.24 \cdot 10^4$	$1.95 \cdot 10^3$
B	4	AZT+3TC+RIT	$2.44 \cdot 10^6$	<9	$5.41 \cdot 10^4$	$6.78 \cdot 10^3$	<7
	24	AZT+3TC+RIT	$7.62 \cdot 10^4$	<11	$5.11 \cdot 10^4$	$1.69 \cdot 10^3$	$8.50 \cdot 10^1$
	48	AZT+3TC+RIT	$6.64 \cdot 10^5$	66	$2.80 \cdot 10^5$	$2.39 \cdot 10^4$	$4.28 \cdot 10^3$
114	0	none	$1.77 \cdot 10^4$	<6	$4.18 \cdot 10^4$	$2.99 \cdot 10^4$	$5.42 \cdot 10^3$
B	4	AZT+3TC	$2.73 \cdot 10^5$	256	$1.92 \cdot 10^4$	$1.79 \cdot 10^4$	$3.00 \cdot 10^1$
	24	AZT+3TC	$1.16 \cdot 10^5$	94	$5.65 \cdot 10^4$	$1.33 \cdot 10^4$	$2.52 \cdot 10^2$
	48	AZT+3TC	$4.26 \cdot 10^4$	47	$6.42 \cdot 10^2$	<1090	$3.22 \cdot 10^2$
119	0	none	$4.94 \cdot 10^5$	63	$1.97 \cdot 10^5$	$1.52 \cdot 10^4$	$3.84 \cdot 10^4$
B	4	AZT+3TC	$3.78 \cdot 10^6$	<55	$1.20 \cdot 10^6$	<11000	$5.90 \cdot 10^2$
	24	AZT+3TC	$6.67 \cdot 10^5$	66	$5.88 \cdot 10^4$	$6.82 \cdot 10^4$	$5.13 \cdot 10^3$
	48	d4T+3TC+NEL (40)	$3.43 \cdot 10^5$	34	$2.83 \cdot 10^3$	<896	$9.00 \cdot 10^1$
302	0	none	$6.29 \cdot 10^5$	114	$7.02 \cdot 10^5$	$3.37 \cdot 10^4$	$2.49 \cdot 10^4$
B	4	AZT+3TC	$5.78 \cdot 10^4$	<29	$6.64 \cdot 10^4$	$4.30 \cdot 10^3$	$8.70 \cdot 10^2$
	24	AZT+3TC	$1.74 \cdot 10^4$	<6	$2.91 \cdot 10^2$	<581	$1.05 \cdot 10^2$
	48	AZT+3TC	<339	<34	$2.09 \cdot 10^3$	<339	$8.24 \cdot 10^2$

*A, without; B, with plasma viral rebound (see Results); FI, fluorescent intensity; LT, lymphoid tissue; ISH, *in situ* hybridization; VL, viral load.

anti-human dendritic reticulum cell (1:20; DAKO), and 5) 5 μg/ml of Cy5-conjugated goat anti-mouse IgM (μ-chain specific, multiple labeling grade; Jackson Immuno Research Laboratories, West Grove, PA) and 0.5 μmol/L of 4′,6-diamidino-2-phenylindole (DAPI; Sigma). All antibody incubations were performed in a dark humidified chamber at room temperature for 30 minutes and were followed by three washes in TNT for 5 minutes. Sections were dehydrated in 70, 90, and 100% ethanol and mounted using ProLong Antifade (Molecular Probes). To assess nonspecific binding, some sections were stained by replacing the anti-p24 antibody with 5 μg/ml of mouse IgG (Sigma).

To verify the linearity of fluorescent intensity quantitation, 10-μm beads coated with well-defined quantities of mouse monoclonal antibody (DAKO Qifikit) were stained in 500 μl of TNB containing 5 μg/ml of Cy3-conjugated goat anti-mouse Ig according to the manufacturer's instructions and then resuspended in 100 μl of water. Twenty microliters of stained bead suspensions were dropped on Superfrost Plus slides and allowed to adhere for 10 minutes. After removing excess fluid by aspiration,

slides were air-dried for 15 minutes and coverslipped. Images of Cy3 fluorescence were acquired through the 40× objective using 100 milliseconds and 1-second exposures. After subtracting the mean gray value of bead-free areas, total gray value (1-second exposure) of individual beads was measured. For beads showing pixel saturation on 1-second exposures, total gray value on the 100-millisecond image was multiplied by 10.

In Situ *Hybridization*

Slides with unfixed sections were warmed to room temperature and fixed for 10 minutes with 4% paraformaldehyde in PBS at room temperature. After two washes in PBS (5 minutes each), sections were permeabilized with 1 μg/ml proteinase K (Boehringer Mannheim, Rotkreuz, Switzerland) in TE (50 mmol/L Tris-HCl, pH 7.5, 10 mmol/L ethylenediaminetetraacetic acid) for 10 minutes at 37°C, washed in PBS, fixed again as above, acetylated for 15 minutes in 0.1 mol/L triethanolamine, pH 8.0, by addition of 0.5% acetic acid anhydride. The slides were then washed twice in PBS (5 minutes), once in 2× standard saline citrate (SSC; 5 minutes) dehydrated in 70, 90, and 100% ethanol (3 minutes each) and air-dried.

The probes, consisting of digoxigenin-labeled RNA derived by *in vitro* transcription of plasmids F, H, I, and J (Lofstrand Labs Ltd., Gaithersburg, MD) and representing 7.8 kb (85%) of the HIV-1 genome, were carbonate-sheared to 350 nucleotides average length. Antisense or sense probe mix was prepared by mixing equimolar amounts of labeled RNA from each of the four plasmids. The probe mix was diluted to 2.5 ng/μl with 2× ISH buffer (Amersham) to which 45% deionized formamide, 5 mmol/L dithiothreitol (Sigma), and 1 U/μl RNase inhibitor (RNAguard; Pharmacia, Uppsala, Sweden) were added. Sections were covered with 20 μl of probe mix under 18 × 18 mm coverslips and hybridized at 50°C overnight in a humid chamber. Slides were subsequently washed twice for 5 minutes in 2× SSC/45% formamide at 45°C, for 15 minutes in 2× SSC at 45°C, for 30 minutes in 2× SSC containing 12.5 μg/ml of RNase A (Boehringer) at 37°C, for 5 minutes in 2× SSC at 37°C, for 10 minutes in 2× SSC at 45°C, and for 5 minutes in 2× SSC at room temperature. Hybridized sections were rinsed in PBS and endogenous peroxidases were inactivated in 3% hydrogen peroxide/PBS for 10 minutes, followed by digoxigenin detection using tyramide signal amplification (Cy3-TSA Direct ISH; NEN) with horseradish peroxidase-conjugated sheep anti-digoxigenin (Boehringer) diluted 1:250 according to the manufacturer's instructions. After counterstaining with DAPI, sections were mounted using ProLong Antifade.

Microscopy and Fluorescent Quantitation

Slides were examined using a Leica DM/RXA epifluorescence microscope equipped with a HBO 100W mercury lamp, four filter cubes (TR1 DAPI, High Q 41001 FITC, High Q 41007a Cy3, and High Q 41008 Cy5; Chroma, Brattleboro, VT) mounted on a motorized wheel, PL Fluotar 40×/0.70 and 10×/0.30 objectives on a motorized nose piece, and a motorized stage (Leica AG, Switzerland). Microscope images were captured with a cooled CCD digital camera (Micromax RTE/CCD 1317-K1, 12 bit; Princeton Instruments, Trenton, NJ), connected to an Intel 586-based computer. MetaMorph Image Analysis software (version 3.5, Universal Imaging Corp., West Chester, PA) was used for microscope control, image acquisition, and image processing. 40× fields showing visible Cy3 reactivity were recorded as dark current-subtracted and shading-corrected 16-bit images with 1-second exposures. For IHC each field was imaged four times to separately record the nuclear (DAPI), CD3 (Alexa488), p24 (Cy3), and FDC (Cy5) fluorescence, and for ISH each field was imaged two times to separately record the nuclear (DAPI) and HIV-1 RNA (Cy3) fluorescence. After background subtraction, specific HIV-related fluorescence (IHC p24 or ISH HIV-1 RNA) was quantified from digital images as fluorescent intensity (gray value), hereafter referred to as fluorescent intensity units (FIU), or positive signal area (number of pixels with intensities above threshold). Montaged images representing an entire section were acquired with the 10× objective and 1-second exposures.

For IHC, binary masks representing CD3- and FDC-positive areas, generated from the Alexa488 and Cy5 images, were used to measure p24-specific fluorescence co-localizing with either CD3 or FDC or both. For ISH, Metamorph standard functions were used to count fluorescent granules on Cy3 images. Briefly, digital image processing involved recalculating the pixel data using Metamorph's "Detect Edges" filter, which employs a Laplace 2 convolution. Next, the convolved image was binarized at a threshold of 200. ISH granule counts were highly correlated with fluorescent intensity and the number of RNA copies, as shown in Results.

HIV-1 RT-PCR

HIV-1 RNA in frozen tissue sections was measured by amplifying extracted, purified total RNA with a quantitative, HIV-1 RT-PCR (Amplicor HIV-1 Monitor Test Kit, Roche Diagnostic Systems, Inc., Branchburg NJ).[36] To calculate HIV-1 RNA copies/mg tissue, total mg of tissue extracted was determined by using morphometry data from sections neighboring those used for extraction. HIV-1 RNA copies/section were calculated by multiplying HIV-1 RNA copies/mg by mg/section, as determined with morphometry.

Plasma VLs were assessed with the Amplicor HIV-1 Monitor Test Kit using ultrasensitive procedures, as previously reported.[36,38]

Statistics

A P value <0.05 was considered significant. Results of linear regressions are reported with r^2. For calculations of the area under the curve and $\log_{10}$ decreases (Δlog), measurements below the quantitation limit were assigned

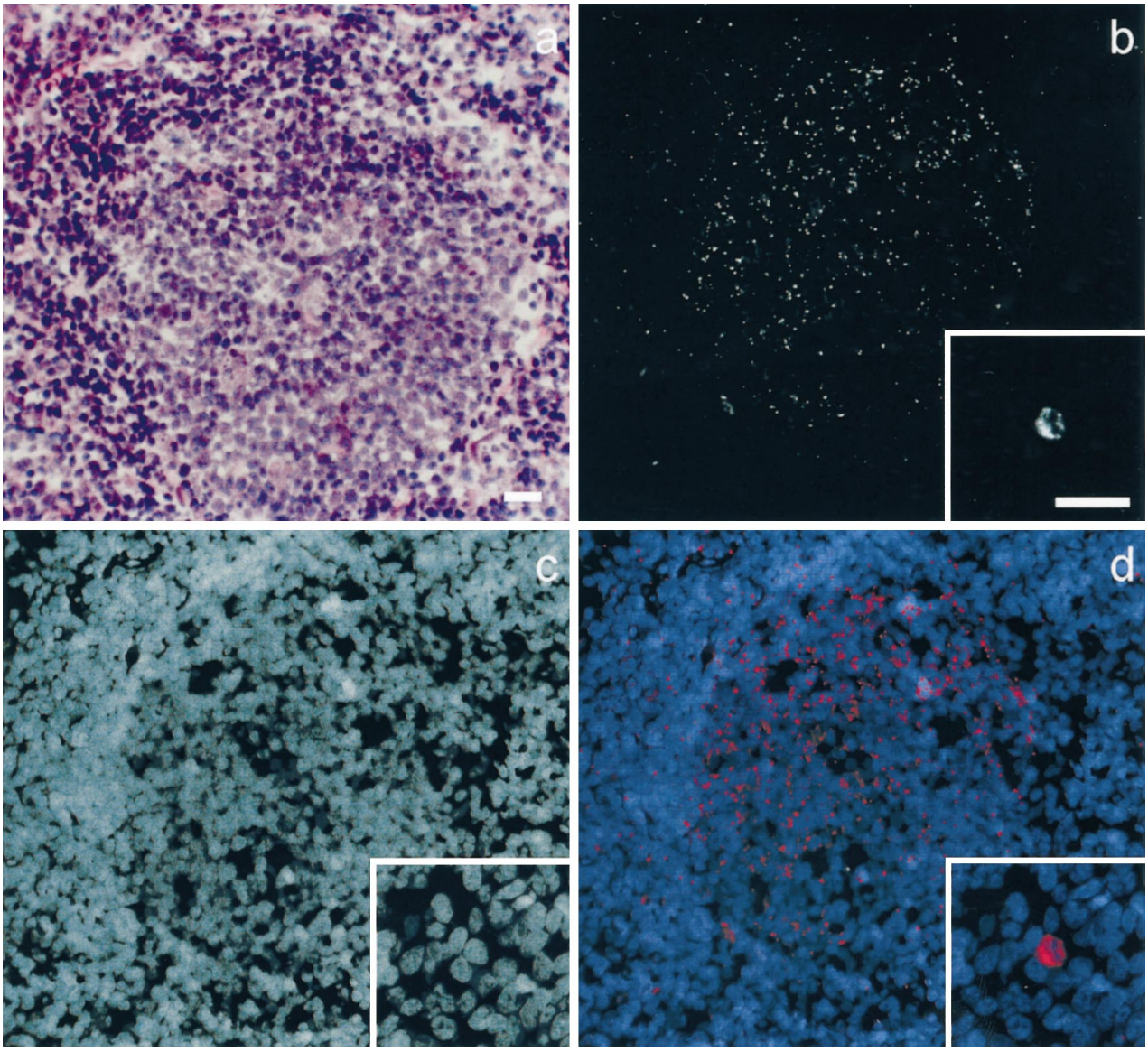

Figure 1. ISH detection of HIV-1 RNA in a tonsil frozen section. Gray scale images display the follicular distribution of HIV-1 RNA (Cy3 fluorescence) (**b**) and an infected cell from a different field (**b, inset**); cell nuclei in the same fields are revealed by DAPI fluorescence (**c**). **d:** An overlay of **b** (colored red) and **c** (colored blue), shows the location of HIV-1 RNA relative to the cell nuclei. The corresponding H&E-stained field from a neighboring section is shown in **a**. Scale bars, 50 μm.

the lower limit of detection, which ranged from 10 to 50 HIV-1 RNA copies per ml plasma.

Results

Morphological Categorization of HIV-1 RNA and p24

HIV-specific fluorescent signals revealed by IHC or ISH were morphologically categorized as either infected cell-associated (intracellular) or diffusely distributed (not clearly within an infected cell). Intracellular signals were clearly localized around or over a nucleus (DAPI-positive) and confined to the expected cell boundaries (Figure 1, insets, and Figure 4f). Diffusely distributed HIV-specific fluorescence, interpreted as extracellular, appeared in ISH as discrete fluorescent granules 0.4 to 2 μm in diameter (Figure 1) and in IHC as fluorescent network over lymphoid follicles (Figures 2 and 4).

HIV-1 p24 Distribution by Cell Type

In all sections examined, intracellular p24 was only found in CD3-positive cells (T lymphocytes). HIV p24 fluorescence identified morphologically as extracellular was further categorized according to co-localization with CD3 and/or FDC cellular markers (Figure 4). Distribution of p24 among the resulting four co-localization categories (co-localization with FDC only, with CD3 only, with FDC and CD3 or with neither cell marker) is summarized in Figure 3. The histological pattern of FDC-associated p24 showed fluorescence spread along the FDC dendritic

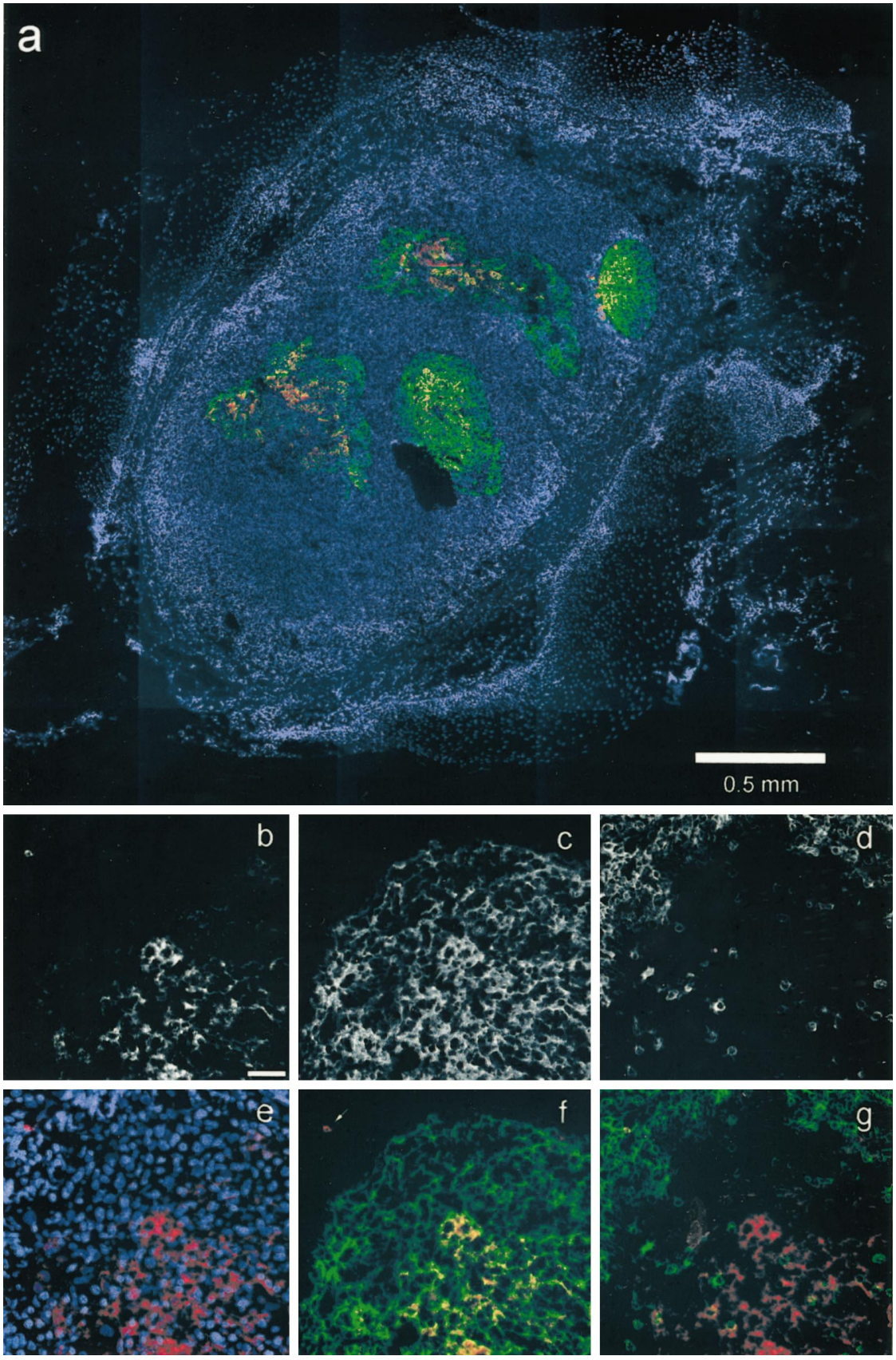
a
0.5 mm
b
c
d
e
f
g

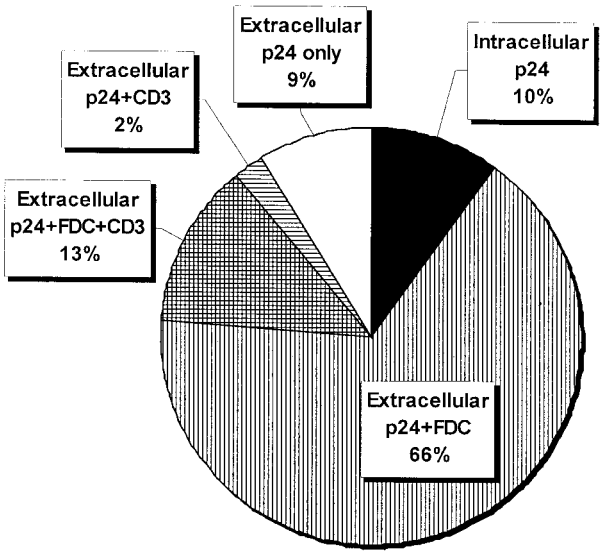

Figure 3. Co-localization of p24 and cell marker fluorescence. Total p24 Fl (**circle**; average of 41 p24-positive biopsies) was subdivided into intracellular (black), extracellular (Xcell) FDC-associated (**vertical lines**), extracellular CD3-associated (**horizontal lines**), extracellular FDC and CD3-associated (**cross-hatch pattern**), and extracellular p24 not otherwise colocalized (white). The FI derived from each subset is indicated as percent of total p24 FI.

processes that encircle lymphocytic cells (Figure 4, e and f). In contrast, CD3-associated p24 typically occurred within the cell's cytoplasm. Applying these histological criteria, most of the p24 in lymphoid follicles that co-localized with both CD3 and FDC seemed to represent FDC-associated virus. The minor fraction of p24-specific signal not co-localizing with any of the cell markers typically lined areas of FDC- or CD3-associated p24 (Figure 4h) and seem to represent thresholding artifacts rather than a unique cellular compartment. In a subset of biopsies, CD68/p24 staining showed that this fraction did not co-localize with CD68-positive cells (data not shown).

Quantitation and Correlation of HIV-1 p24 and HIV-1 RNA in Lymphoid Tissue

To determine the relationship between IHC-derived Cy3 fluorescent intensity and the number of primary antibody binding sites (targets), beads coated with defined numbers of mouse IgG molecules were evaluated by IHC. The six bead types with different surface concentrations were clearly distinguishable on the basis of fluorescent intensity. Linear regression of FIU/bead *versus* bound IgG targets per bead demonstrated an excellent correlation ($r^2 = 0.94$), with a slope of 119 FIU/target and an intercept of 1.08×10^5. These data validated the use of IHC fluorescent intensity as a continuous variable related to the number of target molecules. ISH quantitations were done by counting fluorescent granules (see Methods). The use of granule counts enhanced quantitative accuracy by reducing the influence of nonspecific background fluorescence. The fluorescent intensity/granule conversion was validated in an analysis of all 50 individual sections that were HIV-1 ISH-positive: granule counts/section (median, 618; range, 32 to 7182) and FIU/section (median, 3.30×10^6; range, 8.39×10^4 to 1.79×10^8) were highly correlated ($r^2 = 0.88$, linear regression).

Quantitations obtained by IHC or ISH were further supported by comparison with the number of HIV-1 RNA copies determined by RT-PCR in tissue sections representing the whole biopsy. Significant correlations between HIV-1 RNA copies/section and ISH HIV-1 RNA granules/section ($r^2 = 0.62$, $P < 0.0001$) or IHC p24 FIU/section ($r^2 = 0.51$, $P = 0.0053$) were found (Figure 5). These relationships were modeled as follows: for IHC, the bead calibration data (described above) was used to derive the formula: $y = 119 * 1500 * 0.5x + 1.08 \times 10^5$, where y = predicted FIUs, 1500 = estimated p24 targets/virion[30] (assuming that all 1500 targets could be labeled by IHC), 0.5 converts HIV-1 RNA copies to HIV-1 virion equivalents (2 HIV-1 RNA copies/virion), and x = HIV-1 RNA copies measured. The predicted relationship is plotted with the data (Figure 5, right panel). The formula shows a good fit to the experimental data ($r^2 = 0.73$, $P < 0.0001$), and the absolute number of IHC-predicted virions is close to the actual number of RT-PCR virion equivalents (slope = 0.88, linear regression) (Figure 5). For ISH, each granule represents a minimum of one virion because the two HIV-1 RNAs in a virion cannot be differentiated at the resolution of light microscopy. The expected ideal relationship therefore is $y = 0.5x$, where y = ISH granules/section and x = RT-PCR copies/section. Most of the ISH data points fell within ± 1 log of the RT-PCR virion equivalents (Figure 5, left panel). The two outliers could not be explained on technical grounds, and are taken as variability inherent in comparing an individual section (ISH) with an average of the entire biopsy (RT-PCR).

The graphs in Figure 5 show that IHC-negative sections usually contained <10 RT-PCR HIV-1 RNA copies, and that ISH-negative sections usually contained <50 PCR HIV-1 RNA copies. These data suggest lower detection limits of approximately 5 RT-PCR virion equivalents per section by IHC and approximately 25 virion equivalents/section by ISH.

Effects of Therapy on Plasma and Tissue VL

The virological responses of HIV-1 both in plasma and lymphoid tissue were more pronounced in the patients initiating triple (AZT + 3TC + ritonavir; $n = 8$) than in those initiating double (AZT + 3TC; $n = 5$) antiretroviral therapy (Table 1). In the triple-therapy group, all patients

Figure 2. IHC detection of HIV-1 p24 and cellular markers. **a:** Color overlay (blue, nuclei; red, p24; green, FDC; red/green combinations appear as orange to yellow) shows an entire section composed of 25 montaged fields (original magnification, ×10). **b–g:** Show the same high-power field of a lymphoid follicle (original magnification, ×40; scale bar in **b**, 50 μm). **b–d:** Black and white images of the p24 (Cy3), FDC (Cy5), and T cell (Alexa488) fluorescent channels. **e–f:** Color overlays, as follows: overlay of nuclei (blue, DAPI) and p24 (red; **e**); nearly complete co-localization (orange to yellow) of p24 (red) and FDC (green) within the follicle, whereas the infected cell (**arrow**) does not co-localize with FDC (**f**); co-localization of the infected cell with CD3 (yellow), no co-localization of CD3 (green) with follicular p24 (red) (**g**).

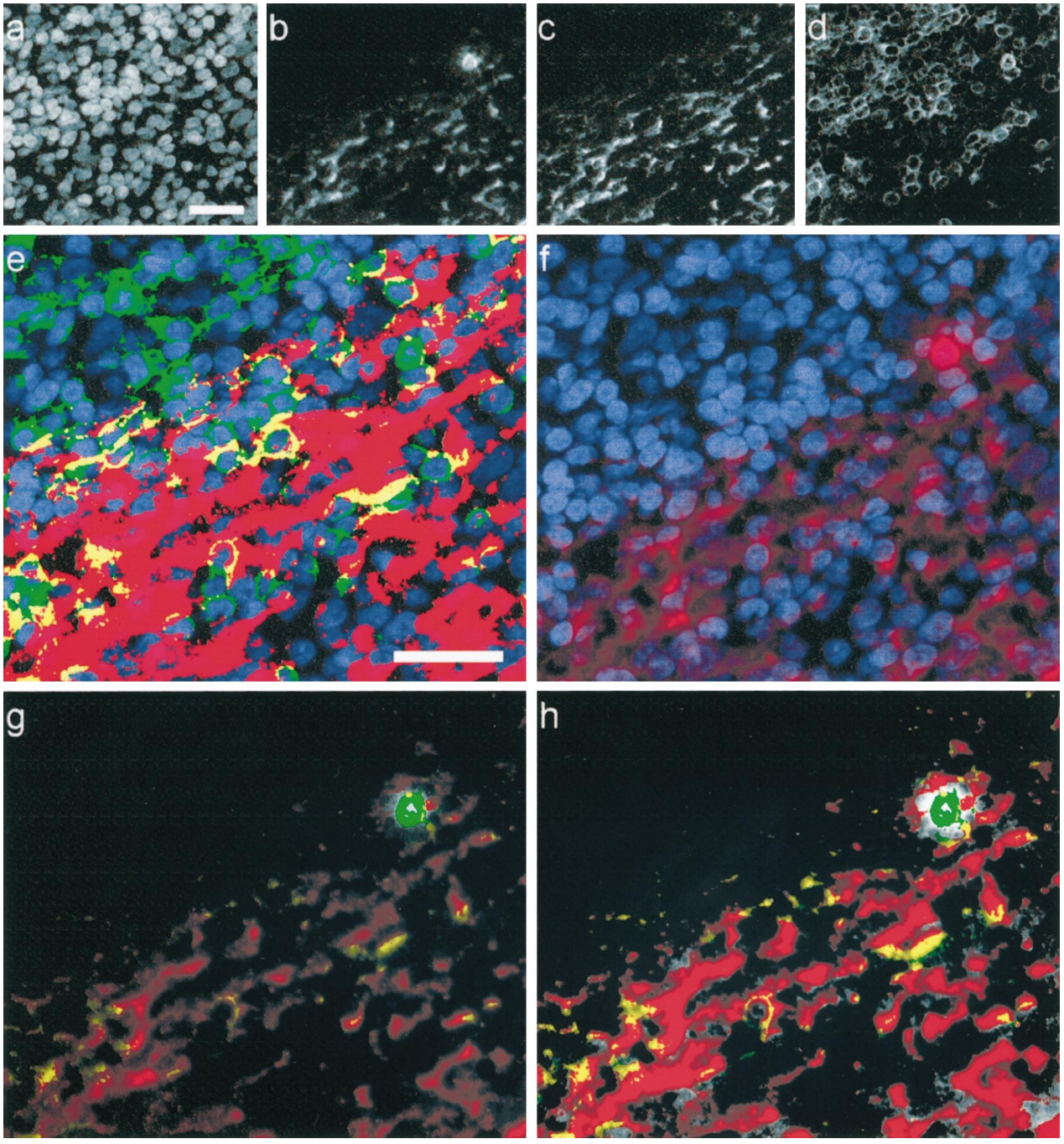

Figure 4. Co-localized subsets of HIV p24 from one field (original magnification, ×40; scale bar, 25 μm). **a–d:** Black and white images of each fluorescent channel: nuclei (DAPI) (**a**), HIV p24 (Cy3) (**b**), FDC (Cy5) (**c**), and T cells (CD3, Alexa488) (**d**). **e:** Nuclei (blue) overlaid with binary masks showing distributions of FDC (red), CD3 (green), or both markers in the same pixel (yellow). **f:** Distribution of p24 (red) relative to cell nuclei (blue). **g:** HIV p24 signal is color encoded according to co-localization with cell markers (color intensity is proportional to fluorescent intensity); p24 + FDC (red), p24 + CD3 (green), p24 + FDC + CD3 (yellow), p24 not colocalized (gray). **h:** For comparison, this contrast-enhanced copy of **g** shows color encoding more clearly.

reached plasma VL <50 copies/ml between weeks 4 and 12. Sustained suppression up to week 48 was observed in five out of eight patients, whereas transient viral replication with plasma VL spikes of 105 to 211 copies/ml occurred in two and viral rebound to pretreatment levels in one patient. In the double-therapy group, in only two of five patients plasma VL dropped below 50 copies/ml at weeks 4 or 12, respectively, but subsequently increased to 824 or 322 copies/ml by week 48, whereas three patients, after an initial drop to 193 to 590 copies/ml, experienced viral rebound to plasma VL more than 1000 copies/ml. Two of those were switched to triple therapy at weeks 24 and 40, respectively, subsequently leading to sustained viral suppression to <50 copies/ml in one and a transient drop to <50 copies/ml followed by rebound to 90 copies/ml in the other.

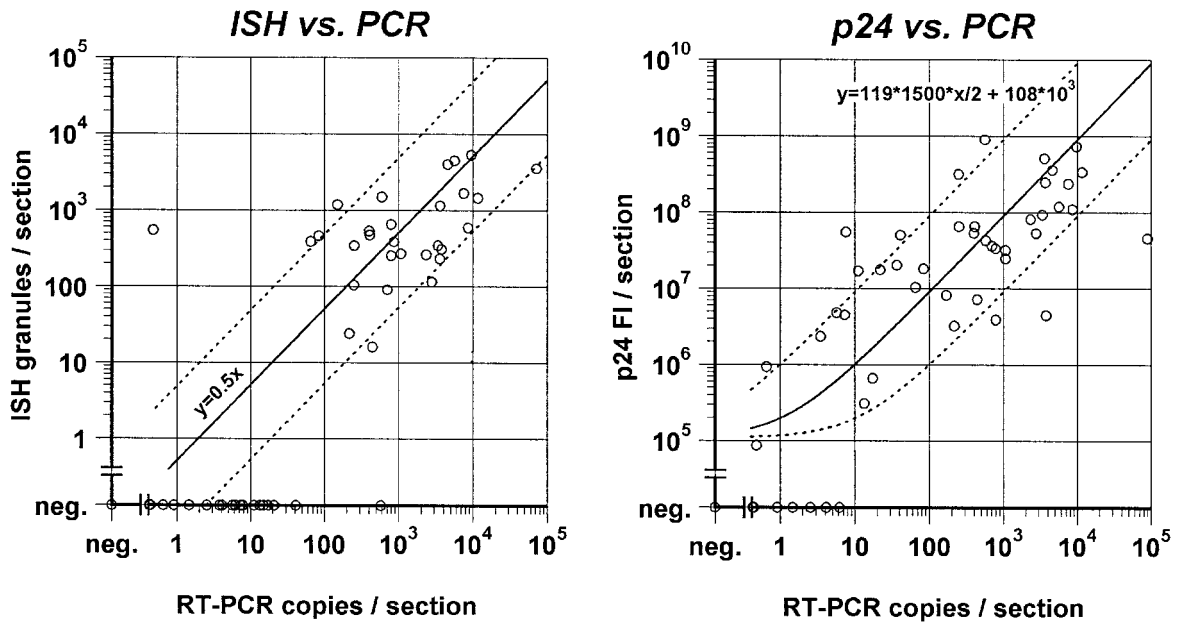

Figure 5. HIV-1 RNA ISH expressed as fluorescent granules per section (**left**) and p24 ICC fluorescent intensity (Fl) per section (**right**) compared with HIV-1 RNA copies/section. **Solid lines** show expected theoretical relationship based on the formulas shown, and **dotted lines** indicate a range of ± 1 $\log_{10}$ (see text for details).

Frozen sections representing every level of a biopsy were combined and evaluated with quantitative HIV-1 RT-PCR. HIV-1 RNA was detected in 48 (96%) of 50 biopsies, whereas HIV-1 RNA was detected in 37 (74%) matched plasma specimens (lower limit of detection <50 copies/ml plasma). Between weeks 0 and 48, the geometric mean plasma and tissue VLs decreased by 3.02 $\log_{10}$ HIV-1 RNA copies/ml and 3.03 $\log_{10}$ HIV-1 RNA/mg tissue, respectively (Table 2). In the triple-therapy subgroup, the decreases in plasma and tissue VLs between weeks 0 and 48 were 3.15 $\log_{10}$ HIV-1 RNA copies/ml plasma and 3.19 $\log_{10}$ HIV-1 RNA/mg tissue, respectively; in the double-therapy group, plasma and tissue VLs decreased by 2.74 $\log_{10}$ HIV-1 RNA copies/ml plasma and 2.75 $\log_{10}$ HIV-1 RNA/mg tissue, respectively.

IHC revealed HIV p24 in 41 (82%) of 50 biopsies, whereas 29 (58%) were HIV-1 RNA-positive by ISH. All 13 biopsies obtained before starting antiretroviral therapy were HIV-positive by both methods (Table 2).

Effects of Therapy on Distribution of HIV-1 in Lymphoid Tissue

Among all biopsies with detectable ISH HIV-1 RNA or p24, 10% of the p24 fluorescence was intracellular and 90% extracellular (Figure 3). For ISH, 7% of the HIV-specific fluorescence was intracellular and 93% extracellular. Despite the 3 log decrease in tissue VL, the average extracellular proportions of p24 and HIV-1 RNA were not significantly different among weeks 0, 4, 24, and 48 of therapy ($P > 0.09$ between all time points for both IHC p24 and ISH HIV-1 RNA, Mann-Whitney *U* test) (Table 2). In analyses of the triple- and double-

Table 2. Viral Loads and Extracellular Proportions of Tissue p24 or HIV-1 RNA

		Viral load ($\log_{10}$ HIV-1 RNA copies)				Extracellular HIV-1 (fluorescent microscopy)			
		per ml plasma		per mg tonsil tissue		IHC (p24)		ISH (HIV-1 RNA)	
Week	Biopsies (N)	Pos. (N)*	VL (90% CI)†	Pos. (N)*	VL (90% CI)†	Pos. (N)*	%Xcell (90% CI)†	Pos. (N)*	%Xcell (90% CI)†
0	13	13	4.11 (0.33)	13	5.08 (0.25)	13	98 (0.7)	13	88 (8.1)
4	13	11	2.10 (0.54)	13	3.74 (0.30)	13	84 (16)	9	99 (0.2)
24	13	8	1.64 (0.71)	12	2.75 (0.67)	9	90 (15)	5	100 (na)‡
48	11	5	1.09 (0.70)	10	2.05 (0.66)	6	82 (27)	2	73 (44)

*Pos. (N), number of samples with detectable HIV-1 RNA or p24.
†90% CI, ± 90% confidence interval; VL, viral load; %Xcell, average percent of detected p24 or HIV-1 RNA that was extracellular (positive specimens only).
‡na, not applicable because SD = 0.

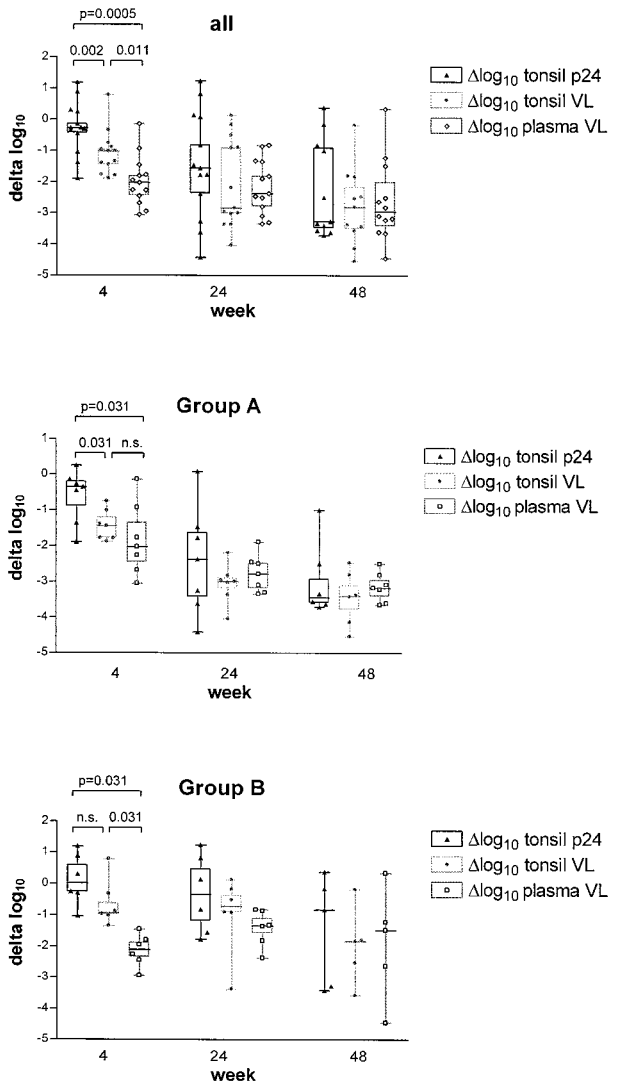

Figure 6. Decreases from baseline in HIV-1 RNA (VL) in plasma, and HIV-1 RNA (VL) and p24 in lymphoid tissue; in all patients (**top**), and in those without (group A) and with (group B) viral rebound during treatment. **Box** and **whiskers** show median, 25th, and 75th percentile and range of the data. n.s., not significant; VL, viral load.

therapy subgroups, there were also no significant differences among time points.

Impact of Incomplete Viral Suppression

To further assess the magnitude of VL reduction in lymphoid tissue between patients with and without complete suppression of HIV-1 RNA in plasma, we divided our study population into two groups: group A consists of seven fully-responding patients without viral rebound (defined as two consecutive measurements of >50 copies/ml after week 12) who were treated with triple therapy, whereas group B represents those with viral rebound and consists of five patients on double and one patient on triple therapy (Table 1 and Figure 6, middle and lower panel). In group A, tonsil p24 became undetectable at week 24 in 4 out of 7 and at week 48 in 4 out of 6 biopsies. An increase in tonsil p24 from week 24 to 48 was observed in two patients on triple-drug regimen, both of which had a single episode of detectable plasma viremia (28 to 105 copies/ml) at week 40. In six out of eight biopsies with negative IHC, RT-PCR detected between 56 and 1040 HIV RNA copies/mg lymphoid tissue, the other two specimens remaining negative. In contrast, p24 remained detectable in tonsils from group B up to week 48 in five of six patients, and the overall decrease in lymphoid tissue HIV-1 RNA was much less pronounced than in group A.

Comparison of Different Assessments of Treatment Response

At baseline, no significant correlations were found between plasma VL, tonsil VL, and tonsil p24, whereas results of ISH correlated with tonsil VL (Pearson r^2 = 0.357; P = 0.03). Correlations between decreases from baseline for plasma VL, tonsil VL, and tonsil p24 are summarized in Figure 7. At week 4, a decrease in plasma VL was observed in all patients. The median change in plasma VL was −2.03 (range, −0.14 to −3.05) $\log_{10}$. In contrast, decrease in tonsil p24 was found in only nine of 13 patients at this time point and with a median of −0.27 $\log_{10}$ was considerably smaller (Wilcoxon signed rank test, P = 0.0018). Similarly, tonsil VL decreased by a median of 1.02 $\log_{10}$ (P = 0.013 *versus* plasma VL). Delta log tonsil p24 correlated with delta log tonsil VL (Pearson r^2 = 0.466; P = 0.010) but not with delta log plasma VL. At weeks 24 and 48, the magnitude of changes from baseline in plasma VL was comparable to those in tonsil VL and p24; all changes correlated now significantly with each other (Figure 7). The delay in primary response in the tonsil compartment is further supported by the observation that both tonsil VL and p24 correlated better with the area under the plasma VL curve during the last 12 weeks before biopsy than with the actual plasma VL at time of biopsy (Figure 8).

Discussion

Highly sensitive visualization of HIV-1 in lymphoid tissues, combined with a novel tissue-sectioning strategy of unfixed frozen tissue sections, enabled us to quantitate the effects of antiretroviral therapy on VL in tissue in asymptomatic individuals with early HIV-1 infection. Full and sustained suppression of viral replication in plasma, achievable in our study population only by triple-combination therapy, led also to a strong reduction of HIV-1 in lymphoid tissue. However, viral p24 or RNA remained almost always detectable in tissue at low concentrations, confirming the inability of the current antiretroviral regimens to completely suppress viral infection.[7,9,10] By comparing the magnitude of HIV-1 decline between plasma and lymphoid tissue in patients on effective triple therapy, the decrease after 4 weeks was more pronounced in plasma than in lymphoid tissue, but reached similar levels at weeks 24 and 48 (Figure 6, group A). This suggests slower decay kinetics in the lymphoid tissue

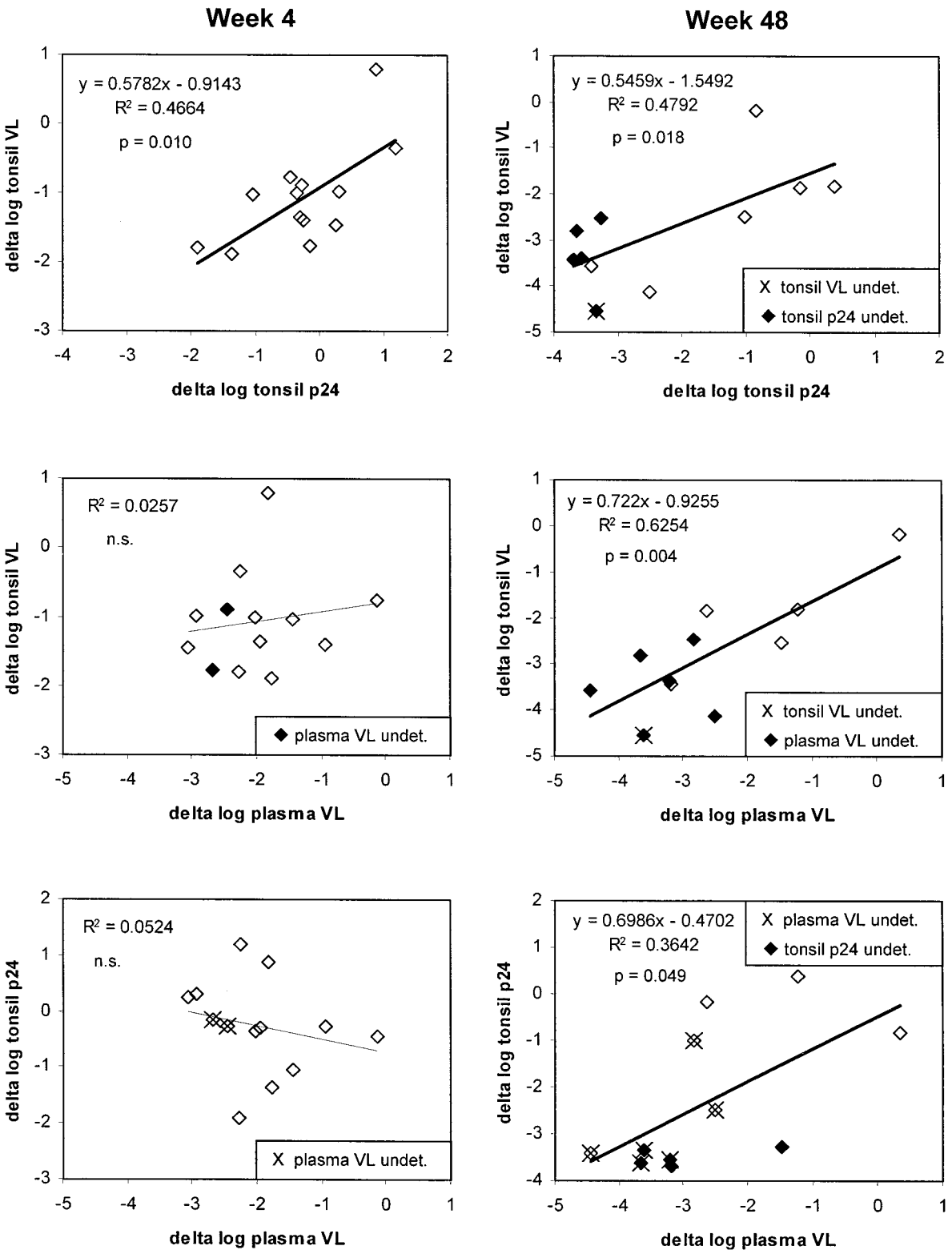

Figure 7. Correlations of decreases from baseline to week 4 (**left**) and 48 (**right**) in HIV-1 RNA (VL) in plasma, and HIV-1 RNA (VL) and p24 in lymphoid tissue. For calculations of $\log_{10}$ decreases, measurements below the detection limit were assigned the lower limit of detection (shown with **solid** data points or marked with **X**; see legend inserts).

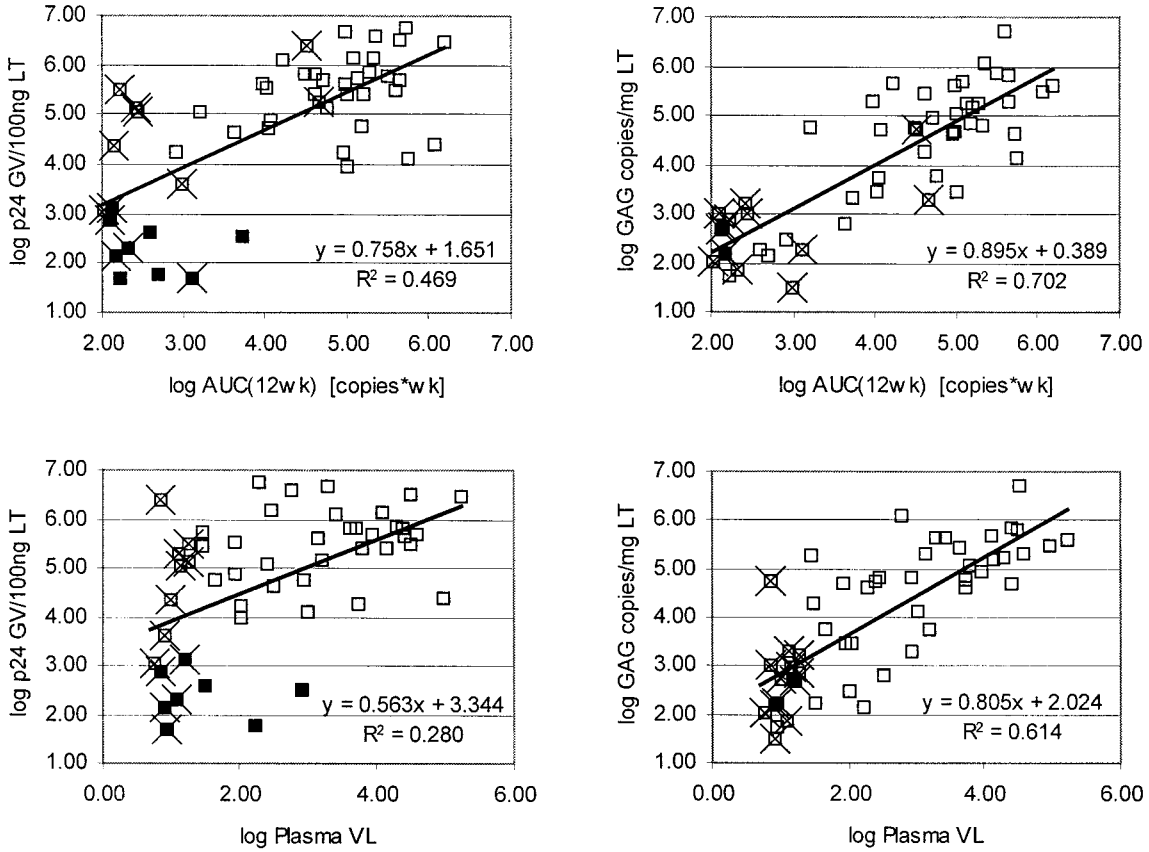

Figure 8. HIV-1 RNA (VL) and p24 in lymphoid tissue correlate better with area under the curve of HIV-1 RNA (VL) in plasma throughout the last 12 weeks before biopsy (**top**) than with the actual plasma HIV-1 RNA (VL) at the time of biopsy (**bottom**). **Solid data points** represent samples with undetectable tonsil p24 (**left**) or tonsil VL (**right**) at the corresponding detection limit, measurements from time points with undetectable plasma VL are marked with **X**. GV, gray value (fluorescent intensity); wk, week; VL, viral load.

compartment, especially if assessed by p24 antigen IHC. Based on this observation and the fact that tonsillar HIV-1 RNA and p24 correlated best with the area under the curve of plasma VL during the last 12 weeks, our results indicate that the amount of FDC-associated virus mirrors the history throughout the last several weeks rather than the current plasma VL.

Overall, we found good correlation between the three different methods applied for the detection of HIV-1 in tissue, namely RT-PCR of HIV-1 RNA per mg of tissue, and quantitative image analysis of HIV-1 RNA determined by ISH, and of p24 antigen determined by IHC. The latter methods have the advantage of allowing precise morphological characterization of cell-associated and cell-free viral particles, but are somewhat less sensitive than RT-PCR (approximated lower detection limits were 5 RT-PCR virion equivalents per section for IHC and 25 RT-PCR virion equivalents per section for ISH). The morphological assessment showed that ~10% of the viral components were associated with infected T lymphocytes, whereas ~90% resided extracellularly on FDC. Furthermore, the average proportions of extracellular to total viral components, measured by p24 IHC and HIV-1 RNA ISH, remained unchanged throughout 1 year of therapy even though plasma and tissue VLs decreased by ~3 logs during the year. This suggests that the rates of therapy-induced reductions in tissue VL are similar in the intracellular and extracellular lymphoid compartments.

Radioactive ISH and image analysis has been used previously to quantify intracellular and extracellular viral RNA in tonsil biopsies.[3,4] Haase et al[3] reported data from 22 tonsil biopsies (7 patients receiving variable antiretroviral treatment with reverse transcriptase inhibitors) in relatively early stages of infection. By recalculating the published data in their Table 1, we determined that they found an average of 94% extracellular (FDC-associated) and 6% mononuclear cell-associated viral RNA, which agrees well with the data reported here. Only four patients in that report had sequential tonsillar biopsies throughout the course of a year and the antiretroviral therapies they received were not effective at reducing the tissue VL. Cavert et al[4] reported similar data from 10 patients with more advanced disease who received highly effective triple-combination therapy and were followed for 24 weeks. In that study, HIV-1-infected mononuclear cells and FDC-associated virus declined in parallel, a finding that is also consistent with our data. They found that at day 2 of triple-combination therapy with AZT, 3TC, and ritonavir, elimination of HIV-1 from FDCs closely followed the rapid decline of VL in tonsillar mononuclear cells and calculated an initial decay half-life of 1.7 days. Between days 2 and 22 they observed slower,

but still parallel decay kinetics in both the FDC and tonsillar mononuclear cell compartment ($t_{1/2}$ ~14 days). Tonsil biopsies that early in therapy were not performed in our patients, but decreases in tonsil VL at weeks 4 and 24 in our triple-therapy patients are in good agreement with the data from that study. Thus, antiretroviral treatment seems to lead to parallel decreases in intracellular and extracellular HIV-1 in lymphoid tissue independent of the stage of HIV infection, even if differences exist regarding the destruction of the follicular dentritic cell network.[39]

In two of our patients on triple therapy, short-term low-level plasma viral rebound was clearly associated with replenishment of FDC-trapped viral antigen. The treatment response in lymphoid tissue was much less pronounced in patients on double-nucleoside analogue therapy, even if their plasma VL remained partially suppressed (frequently between 100 and 1000 HIV-1 RNA copies/ml plasma). This is in agreement with data of Ruiz et al[40] who recently reported high levels of FDC-trapped virions in patients on double-nucleoside analogue therapy despite adequate suppression of HIV-1 RNA in plasma, possibly explained by an inferior ability of double-combination therapy to suppress residual viral replication in lymphoid tissue. The resulting danger of resistance development[41] supports the concept that sustained, maximum viral suppression should be targeted using triple-antiretroviral therapy, even in patients with early HIV infection and good prognostic markers.

We have previously reported the impact of antiretroviral therapy on T-lymphocyte populations in the peripheral blood in the patients of this study.[37,42] Triple therapy led to a higher increase in $CD4^+$ T cells and to stronger decline in CD8+ T cells than double-nucleoside analogue therapy. Triple therapy-induced decrease in plasma HIV RNA levels additionally led to significant reductions in numbers of activated $CD4^+$/HLA-DR+, CD8+/HLA-DR+, and CD8+/CD38+ T cells, as well as in numbers of memory CD8+/CD45RO+ T cells, which contrasted with a concomitant significant increase in numbers of naive $CD4^+$/CD45RA+ and memory $CD4^+$/CD45RO+ T cells. Although changes in T-cell subsets in tonsils were not investigated in our study, disease-associated $CD4^+$ T-cell depletion in the lymphoid tissue is not expected during asymptomatic, early HIV infection,[43] whereas in more advanced disease, where $CD4^+$/CD45RA+ subsets are reduced in lymphoid tissue, it has been shown that triple therapy resulted in sustained increases in the proportion of naive $CD4^+$ T cells in lymphoid tissue to approximately half the normal level.[44]

The application of multicolor fluorescent IHC in this report allowed us to substantiate the differentiation between lymphocytic and FDC-associated HIV-1 by co-localization with cellular markers while quantitating the virus in the same preparation. Using multiple exposures and image analysis techniques, 66% of the extracellular p24 was clearly FDC-associated, 13% was associated with both CD3 and FDC markers, 2% with CD3 alone, and another 9% did not co-localize with either marker. We cannot rule out the possibility that some of the extracellular CD3-associated virus was within lymphocytes. However, this part of the extracellular p24 had a histological pattern consistent with the trabecular network of FDC cytoplasmic extensions. In these 50 biopsies, all of the infected cells detected by IHC were CD3-positive lymphocytes (cell markers were not available for ISH). In separate experiments, we did not find infected CD68 cells, which is consistent with the relative rarity of infected macrophages.[2,45]

In summary, HIV-1 RNA and p24 were quantitatively evaluated by fluorescent microscopy, the fluorescent signals were effectively categorized by morphological and co-localization criteria, and estimates of sensitivity suggested that individual virions were visualized. Typically, ~90% of lymphoid tissue virus is associated with FDC, the remainder residing mostly in T lymphocytes. Analyses showed that the tissue distribution of HIV-1 was independent of tissue VL more than three orders of magnitude. We observed a delayed treatment response of tissue HIV-RNA compared to plasma VL and, even more pronounced, tissue p24, and found that the amount of FDC-associated virus mirrors the history over weeks rather than the current plasma VL. Antiretroviral therapy thus is capable of effectively reducing the amount of HIV-1 in all compartments of the lymphoid tissue, provided that triple-combination therapy is used and full viral suppression in plasma is achieved. However, complete abolition of residual HIV-1 replication is not possible, even if treatment starts early during asymptomatic HIV infection.

Acknowledgments

We thank Roberto Speck for discussions and review of the manuscript; Noelia Berther and Friederike Burgener for skilled technical assistance; and Christina Grube, Dr. Manuel Battegay and Dr. Pietro L. Vernazza for patient management.

References

1. Pantaleo G, Graziosi C, Butini L, Pizzo PA, Schnittman SM, Kotler DP, Fauci AS: Lymphoid organs function as major reservoirs for human immunodeficiency virus. Proc Natl Acad Sci USA 1991, 88:9838–9842
2. Pantaleo G, Graziosi C, Demarest JF, Butini L, Montroni M, Fox CH, Orenstein JM, Kotler DP, Fauci AS: HIV infection is active and progressive in lymphoid tissue during the clinically latent stage of disease. Nature 1993, 362:355–358
3. Haase AT, Henry K, Zupancic M, Sedgewick G, Faust RA, Melroe H, Cavert W, Gebhard K, Staskus K, Zhang ZQ, Dailey PJ, Balfour-HHJ, Erice A, Perelson AS: Quantitative image analysis of HIV-1 infection in lymphoid tissue. Science 1996, 274:985–989
4. Cavert W, Notermans DW, Staskus K, Wietgrefe SW, Zupancic M, Gebhard K, Henry K, Zhang ZQ, Mills R, McDade H, Schuwirth CM, Goudsmit J, Danner SA, Haase AT: Kinetics of response in lymphoid tissues to antiretroviral therapy of HIV-1 infection. Science 1997, 276:960–964
5. Wong JK, Gunthard HF, Havlir DV, Zhang ZQ, Haase AT, Ignacio CC, Kwok S, Emini E, Richman DD: Reduction of HIV-1 in blood and lymph nodes following potent antiretroviral therapy and the virologic correlates of treatment failure. Proc Natl Acad Sci USA 1997, 94:12574–12579
6. Tenner RK, Stellbrink HJ, van Lunzen J, Schneider C, Jacobs JP, Raschdorff B, Grosschupff G, Steinman RM, Racz P: The unenlarged lymph nodes of HIV-1-infected, asymptomatic patients with high CD4 T cell counts are sites for virus replication and CD4 T cell proliferation. The impact of highly active antiretroviral therapy. J Exp Med 1998, 187:949–959
7. Furtado MR, Callaway DS, Phair JP, Kunstman KJ, Stanton JL, Macken CA, Perelson AS, Wolinsky SM: Persistence of HIV-1 tran-

scription in peripheral-blood mononuclear cells in patients receiving potent antiretroviral therapy. N Engl J Med 1999, 340:1614–1622
8. Gunthard HF, Frost SD, Leigh-Brown AJ, Ignacio CC, Kee K, Perelson AS, Spina CA, Havlir DV, Hezareh M, Looney DJ, Richman DD, Wong JK: Evolution of envelope sequences of human immunodeficiency virus type 1 in cellular reservoirs in the setting of potent antiviral therapy. J Virol 1999, 73:9404–9412
9. Romano L, Venturi G, Catucci M, De Milito A, Valensin PE, Zazzi M: Evaluation of cell-free and cell-associated peripheral blood human immunodeficiency virus type 1 RNA response to antiretroviral therapy. J Infect Dis 1999, 179:361–366
10. Dornadula G, Zhang H, VanUitert B, Stern J, Livornese LJ, Ingerman MJ, Witek J, Kedanis RJ, Natkin J, DeSimone J, Pomerantz RJ: Residual HIV-1 RNA in blood plasma of patients taking suppressive highly active antiretroviral therapy. JAMA 1999, 282:1627–1632
11. Zhang L, Ramratnam B, Tenner RK, He Y, Vesanen M, Lewin S, Talal A, Racz P, Perelson AS, Korber BT, Markowitz M, Ho DD: Quantifying residual HIV-1 replication in patients receiving combination antiretroviral therapy. N Engl J Med 1999, 340:1605–1613
12. Yerly S, Rutschmann OT, Opravil M, Marchal F, Hirschel B, Perrin L: Cell-associated HIV-1 RNA in blood as indicator of virus load in lymph nodes. The Swiss HIV Cohort Study. J Infect Dis 1999, 180:850–853
13. Fox CH, Tenner RK, Racz P, Firpo A, Pizzo PA, Fauci AS: Lymphoid germinal centers are reservoirs of human immunodeficiency virus type 1 RNA. J Infect Dis 1991, 164:1051–1057
14. Spiegel H, Herbst H, Niedobitek G, Foss HD, Stein H: Follicular dendritic cells are a major reservoir for human immunodeficiency virus type 1 in lymphoid tissues facilitating infection of CD4+ T-helper cells. Am J Pathol 1992, 140:15–22
15. Heath SL, Tew JG, Szakal AK, Burton GF: Follicular dendritic cells and human immunodeficiency virus infectivity. Nature 1995, 377:740–744
16. Joling P, Bakker LJ, Van SJ, Meerloo T, de Graaf L, Dekker ME, Goudsmit J, Verhoef J, Schuurman HJ: Binding of human immunodeficiency virus type-1 to follicular dendritic cells *in vitro* is complement dependent. J Immunol 1993, 150:1065–1073
17. Schmitz J, van Lunzen J, Tenner RK, Grossschupff G, Racz P, Schmitz H, Dietrich M, Hufert FT: Follicular dendritic cells retain HIV-1 particles on their plasma membrane, but are not productively infected in asymptomatic patients with follicular hyperplasia. J Immunol 1994, 153:1352–1359
18. Fujiwara M, Tsunoda R, Shigeta S, Yokota T, Baba M: Human follicular dendritic cells remain uninfected and capture human immunodeficiency virus type 1 through CD54-CD11a interaction. J Virol 1999, 73:3603–3607
19. Parmentier HK, van Wichen D, Sie Go DM, Goudsmit J, Borleffs JC, Schuurman HJ: HIV-1 infection and virus production in follicular dendritic cells in lymph nodes. A case report, with analysis of isolated follicular dendritic cells. Am J Pathol 1990, 137:247–251
20. Tacchetti C, Favre A, Moresco L, Meszaros P, Luzzi P, Truini M, Rizzo F, Grossi CE, Ciccone E: HIV is trapped and masked in the cytoplasm of lymph node follicular dendritic cells. Am J Pathol 1997, 150:533–542
21. Soontornniyomkij V, Wang G, Kapadia SB, Achim CL, Wiley CA: Confocal microscopy assessment of lymphoid tissues with follicular hyperplasia from patients infected with human immunodeficiency virus type 1. Arch Pathol Lab Med 1998, 122:534–538
22. Tenner RK, Racz P, Bofill M, Schulz MA, Dietrich M, Kern P, Weber J, Pinching AJ, Veronese DF, Popovic M: HTLV-III/LAV viral antigens in lymph nodes of homosexual men with persistent generalized lymphadenopathy and AIDS. Am J Pathol 1986, 123:9–15
23. Biberfeld P, Chayt KJ, Marselle LM, Biberfeld G, Gallo RC, Harper ME: HTLV-III expression in infected lymph nodes and relevance to pathogenesis of lymphadenopathy. Am J Pathol 1986, 125:436–442
24. Frankel SS, Tenner RK, Racz P, Wenig BM, Hansen CH, Heffner D, Nelson AM, Pope M, Steinman RM: Active replication of HIV-1 at the lymphoepithelial surface of the tonsil. Am J Pathol 1997, 151:89–96
25. Cohen OJ, Pantaleo G, Lam GK, Fauci AS: Studies on lymphoid tissue from HIV-infected individuals: implications for the design of therapeutic strategies. Springer Semin Immunopathol 1997, 18:305–322
26. Wenig BM, Thompson LD, Frankel SS, Burke AP, Abbondanzo SL, Sesterhenn I, Heffner DK: Lymphoid changes of the nasopharyngeal and palatine tonsils that are indicative of human immunodeficiency virus infection. A clinicopathologic study of 12 cases. Am J Surg Pathol 1996, 20:572–587
27. Reux I, Fillet AM, Fournier JG, Agut H, Gentilini M, LeHoang P, Hauw JJ: *In situ* hybridization of HIV-1 RNA in retinal vascular wall. Am J Pathol 1993, 143:1275–1279
28. Pezzella M, Pezzella F, Galli C, Macchi B, Verani P, Sorice F, Baroni CD: *In situ* hybridization of human immunodeficiency virus (HTLV-III) in cryostat sections of lymph nodes of lymphadenopathy syndrome patients. J Med Virol 1987, 22:135–142
29. Baroni CD, Pezzella F, Pezzella M, Macchi B, Vitolo D, Uccini S, Ruco LP: Expression of HIV in lymph node cells of LAS patients. Immunohistology, *in situ* hybridization, and identification of target cells. Am J Pathol 1988, 133:498–506
30. Kure K, Lyman WD, Weidenheim KM, Dickson DW: Cellular localization of an HIV-1 antigen in subacute AIDS encephalitis using an improved double-labeling immunohistochemical method. Am J Pathol 1990, 136:1085–1092
31. Lawrence JB, Marselle LM, Byron KS, Johnson CV, Sullivan JL, Singer RH: Subcellular localization of low-abundance human immunodeficiency virus nucleic acid sequences visualized by fluorescence *in situ* hybridization. Proc Natl Acad Sci USA 1990, 87:5420–5424
32. Spadoro JP, Payne H, Lee Y, Rosenstraus MJ: Single copies of HIV proviral DNA detected by fluorescent *in situ* hybridization. Biotechniques 1990, 9:186–195
33. Dirks RW, van de Rijke FM, Fujishita S, van der Ploeg M, Raap AK: Methodologies for specific intron and exon RNA localization in cultured cells by haptenized and fluorochromized probes. J Cell Sci 1993, 104: 1187–1197
34. Patterson BK, Jiyamapa D, Mayrand E, Hoff B, Abramson R, Garcia PM: Detection of HIV-1 DNA in cells and tissue by fluorescent *in situ* 5′-nuclease assay (FISNA). Nucleic Acids Res 1996, 24:3656–3658
35. Andersson J, Fehniger TE, Patterson BK, Pottage J, Agnoli M, Jones P, Behbahani H, Landay A: Early reduction of immune activation in lymphoid tissue following highly active HIV therapy. AIDS 1998, 12: F123–F129
36. Fischer M, Huber W, Kallivroussis A, Ott P, Opravil M, Lüthy R, Weber R, Cone RW: Highly sensitive methods for quantitation of human immunodeficiency virus type 1 RNA from plasma, cells, and tissues. J Clin Microbiol 1999, 37:1260–1264
37. Opravil M, Cone RW, Fischer M, Vernazza PL, Bassetti S, Lorenzi P, Bisset LR, Ott P, Huber W, Knuchel MC, Roos M, Lüthy R, Weber R: Effects of early antiretroviral treatment on HIV-1 RNA in blood and lymphoid tissue: a randomized trial of double *versus* triple therapy. J Acquir Immune Defic Syndr 2000, 23:17–25
38. Schockmel GA, Yerly S, Perrin L: Detection of low HIV-1 RNA levels in plasma. J Acquir Immune Defic Syndr Hum Retrovirol 1997, 14:179–183
39. Zhang ZQ, Schuler T, Cavert W, Notermans DW, Gebhard K, Henry K, Havlir DV, Gunthard HF, Wong JK, Little S, Feinberg MB, Polis MA, Schrager LK, Schacker TW, Richman DD, Corey L, Danner SA, Haase AT: Reversibility of the pathological changes in the follicular dendritic cell network with treatment of HIV-1 infection. Proc Natl Acad Sci USA 1999, 96:5169–5172
40. Ruiz L, van Lunzen J, Arno A, Stellbrink HJ, Schneider C, Rull M, Castella E, Ojanguren I, Richman DD, Clotet B, Tenner RK, Racz P: Protease inhibitor-containing regimens compared with nucleoside analogues alone in the suppression of persistent HIV-1 replication in lymphoid tissue. AIDS 1999, 13:F1–F8
41. Gunthard HF, Wong JK, Ignacio CC, Guatelli JC, Riggs NL, Havlir DV, Richman DD: Human immunodeficiency virus replication and genotypic resistance in blood and lymph nodes after a year of potent antiretroviral therapy. J Virol 1998, 72:2422–2428
42. Bisset LR, Cone RW, Huber W, Battegay M, Vernazza PL, Weber R, Grob PJ, Opravil M: Highly active antiretroviral therapy during early HIV infection reverses T-cell activation and maturation abnormalities. Swiss HIV Cohort Study. AIDS 1998, 12:2115–2123
43. Rosok BI, Bostad L, Voltersvik P, Bjerknes R, Olofsson J, Asjo B, Brinchmann JE: Reduced CD4 cell counts in blood do not reflect CD4 cell depletion in tonsillar tissue in asymptomatic HIV-1 infection. AIDS 1996, 10:F35–F38
44. Zhang ZQ, Notermans DW, Sedgewick G, Cavert W, Wietgrefe S, Zupancic M, Gebhard K, Henry K, Boies L, Chen Z, Jenkins M, Mills R, McDade H, Goodwin C, Schuwirth CM, Danner SA, Haase AT: Kinetics of CD4+ T cell repopulation of lymphoid tissues after treatment of HIV-1 infection. Proc Natl Acad Sci USA 1998, 95:1154–1159
45. Haase AT: Population biology of HIV-1 infection: viral and CD4+ T cell demographics and dynamics in lymphatic tissues. Annu Rev Immunol 1999, 17:625–656